Inorganic Chemistry
Article

*Inorg. Chem.* **2009**, *48*, 9365–9376 **9365**
DOI: 10.1021/ic901191a

# Structural and NMR Characterization of Sm(III), Eu(III), and Yb(III) Complexes of an Amide Based Polydentate Ligand Exhibiting Paramagnetic Chemical Exchange Saturation Transfer Abilities

**Jason D. Dorweiler,[†] Victor N. Nemykin,[†] Amanda N. Ley,[‡] Robert D. Pike,[‡] and Steven M. Berry*[,†]**

[†]*Department of Chemistry and Biochemistry, University of Minnesota Duluth, 1039 University Drive, Duluth, Minnesota 55812-3020, and* [‡]*Department of Chemistry, College of William and Mary, P.O. Box 8795, Williamsburg, Virginia 23187-8795*

Received June 20, 2009

Complexes of Sm(III), Eu(III), and Yb(III) with a new polydentate ether ligand with amide arms were synthesized. Solid state X-ray structures of the complexes reveal all three complexes crystallize in monoclinic unit cells. The mononuclear complexes have nine coordinate tricapped trigonal prismatic geometries with coordination of all four amide carbonyl oxygen and all three of the backbone ether oxygen atoms. The molecules possess a pseudo $C_2$ symmetry axis. The complexes were characterized by solution and solid state emission spectroscopy and IR spectroscopy. Solution state behavior of the complexes was further explored using NMR. The $^1$H NMR spectra show 16 peaks suggesting the complexes are slow in exchanging on the NMR time scale and that the $C_2$ symmetry axis is maintained. The NMR spectra were assigned using $^1$H, $^{13}$C, COSY, and HMQC experiments. The Eu(III) complex was tested for the recently explored Magnetic Resonance Imaging phenomenon called paramagnetic chemical exchange saturation transfer (PARACEST). At physiological pH and temperature two CEST peaks were observed that caused a decrease in the bulk water molecule signal intensity of 10 and 16%.

## Introduction

Lanthanide (Ln) complexes have a wide range of interesting applications exploiting their luminescent and magnetic properties.[1] They are investigated for uses in areas such as catalysts for organic reactions,[2] photosensitive glasses,[3] sensors,[4−6] and NMR shift reagents.[7,8] A particularly interesting application of Ln complexes is their *in vivo* use as imaging reagents through fluorescence imaging,[9−11] as well as Magnetic Resonance Imaging (MRI) contrast reagents.[12−16] Complexes can be injected into a tissue of interest, or ligands with cell permeable groups can allow imaging of specific tissue types.[16] Since these complexes are used in cells it is exceedingly important that the complexes are both kinetically and thermodynamically stable especially under aqueous physiological conditions since free Ln ions are toxic.[14,17] One strategy to avoid the dissociation of lanthanide ions in solution is to employ complexes with large chelating polydentate ligands that occupy several of the Ln coordination sites. The addition of hydrophobic end groups to the ligands can also help reduce the absorption of Ln complexes and aid in their excretion.[16]

For MRI applications, the magnetic field derived from paramagnetic Ln ions is used to alter the relaxivity of the protons on coordinating water molecules from the tissue. MRI reagents typically work by altering the $T_1$ or $T_2$ relaxation

*To whom correspondence should be addressed. E-mail: smberry@d.umn.edu. Phone: +1 218 726 7087. Fax: +1 218 726 7394.

(1) *Handbook on the Physics and Chemistry of Rare Earths*; Gschneidner, K. A., Jr., Bünzli, J.-C. G., Pecharsky, V. K., Eds.; Elsevier: Amsterdam, The Netherlands, 2009; Vol. *39*, p 445 ff.
(2) Sloan, L. A.; Procter, D. J. *Chem. Soc. Rev.* **2006**, *35*, 1221–1229.
(3) Adam, J.-L. *Chem. Rev.* **2002**, *102*, 2461–2476.
(4) Montgomery, C. P.; Murray, B. S.; New, E. J.; Pal, R.; Parker, D. *Acc. Chem. Res.* **2009**, *42*, 925–937.
(5) Song, B.; Wang, G.; Tan, M.; Yuan, J. *J. Am. Chem. Soc.* **2006**, *128*, 13442–13450.
(6) Parker, D.; Senanayake, P. K.; Williams, J. A. G. *J. Chem. Soc., Perkin Trans. 2* **1998**, 2129–2139.
(7) Wenzel, T. J.; Wenzel, B. T. *Chirality* **2008**, *21*, 6–10.
(8) Komarov, I. V.; Nemykin, V. N.; Subbotin, N. B. *Appl. Magn. Reson.* **1993**, *4*, 377–382.
(9) Bornhop, D. J.; Hubbard, D. S.; Houlne, M. P.; Adair, C.; Kiefer, G. E.; Pence, B. C.; Morgan, D. L. *Anal. Chem.* **1999**, *71*, 2607–2615.
(10) Bornhop, D. J.; Griffin, J. M. M.; Goebel, T. S.; Sudduth, M. R.; Bell, B.; Motamedi, M. *Appl. Spectrosc.* **2003**, *57*, 1216–1222.
(11) Moore, E. G.; Samuel, A. P. S.; Raymond, K. N. *Acc. Chem. Res.* **2009**, *42*, 542–552.
(12) Aime, S.; Crich, S. G.; Gianolio, E.; Giovenzana, G. B.; Tei, L.; Terreno, E. *Coord. Chem. Rev.* **2006**, *250*, 1562–1579.
(13) Frey, S. T.; Chang, C. A.; Carvalho, J. F.; Varadarajan, A.; Schultze, L. M.; Pounds, K. L.; Horrocks, W. D., Jr. *Inorg. Chem.* **1994**, *33*, 2882–2889.
(14) Bellin, M.-F. *Eur. J. Radiol.* **2006**, *60*, 314–323.
(15) Bottrill, M.; Kwok, L.; Long, N. J. *Chem. Soc. Rev.* **2006**, *35*, 557–571.
(16) Misra, S. N.; Gagnani, M. A.; Devi, I. M.; Shukla, R. S. *Bioinorg. Chem. Appl.* **2004**, *2*, 155–192.
(17) Pandya, S.; Yu, J.; Parker, D. *Dalton. Trans.* **2006**, 2757–2766.


Published on Web 08/27/2009

**Scheme 1.** General Structure of the Ln(III) Complexes of **L** with Labeling of the Protons for NMR Assignments[a]

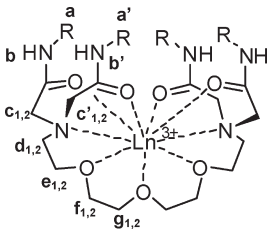


[a] Ln(III) = Eu(III), Sm(III), or Yb(III) ions.

rates of the nearby water molecules.[12] These mechanisms are aided by allowing water molecules to bind the metal atom. It is advantageous therefore for a complex to have an inner sphere coordination site for a water molecule to bind.[18] The design of a functional MRI reagent must therefore consider both the availability of water coordination sites and also the inertness of the complex under physiological conditions.[19]

A newer class of MRI contrast reagents has recently been identified based on a different mechanism called chemical exchange saturation transfer (CEST).[20] These reagents function by chemical exchange of a proton on the ligand that can be saturated by a radiofrequency pulse and then exchanged with the bulk water molecules. The mechanism of this is described in more detail by Woods et al.[21] Since CEST depends on chemical exchange it is not important that the contrast reagent have an open binding site for water. Furthermore, CEST reagents utilizing paramagnetic nuclei, referred to as PARACEST reagents, are potentially more effective for generating CEST contrast.[21] This different contrast mechanism can be useful for pH mapping of different tissues,[22] and detection of proteins,[23,24] metabolites,[25−27] and temperature.[28]

In the present paper, we report the successful synthesis of a new polydentate amide based ligand (Scheme 1) and coordination of this ligand with Sm(III), Eu(III), and Yb(III) ions. The large chelating ligand was designed with four arms to wrap around Ln(III) ions, to allow ready modification of ligand side groups, and to contain exchangeable protons. In addition to this it has seven oxygen donor atoms (four carbonyl and three ether) available for bonding as well as two nitrogen donors. The large availability of donor atoms in the ligand help increase its solution stability. The synthesis of the ligand along with the characterization of its Sm(III), Eu(III), and Yb(III) complexes by X-ray crystallography, NMR, and luminescence are described. Finally, on the basis of the presence of exchangeable protons and the solution stability of the complex, we characterized its potential MRI PARACEST applications.

## Experimental Section

**Materials.** Solvents and reagents were of commercial grade and used without further purification. Hexahydrates of Eu(III) and Sm(III) nitrates and the pentahydrate of Yb(III) nitrate were obtained from Strem Chemicals.

**Synthesis.** The ligand and complex were prepared in an analogous fashion to published literature procedures with modifications as described below.

**Tetraethyleneglycol Ditosylate (1).**[29] Pyridine (250 mL) was added to 19.4 g (0.10 mol) of tetraethylene glycol. The mixture was cooled to −10 °C for the duration of the reaction. Tosyl chloride (58.5 g, 0.28 mol, 2.8 mol eq.) was dissolved in 250 mL of pyridine and added dropwise under argon for 3 h. After addition of the tosyl chloride the reaction mixture was stirred for another 3 h. The resulting precipitated white byproduct (pyridine HCl) was removed by filtration. Ice cold water (∼250 mL) was added to the filtrate, and it was extracted with dichloromethane (3 × 250 mL). The organic layer was then washed several times with 6 M HCl until the volume of the organic layer stopped decreasing, followed by saturated ammonium chloride solution (1 × 250 mL). The organic layer was dried with sodium sulfate, and the solvent was evaporated to give a light yellow oil (overall yield: 38.3 g, 76%). $^1$H NMR (300 MHz, $CDCl_3$, 25 °C, TMS), $\delta$(ppm) = 2.45 (s, 6H), 3.56 (s, 8H), 3.68 (t, 4H), 4.15 (t, 4H), 7.31 (d, 4H), 8.02 (d. 4H). $^{13}C\{^1H\}$ NMR (500 MHz, $CDCl_3$, 25 °C, TMS) $\delta$(ppm) 21.91 ($CH_3$), 68.95 ($CH_2$), 69.51 ($CH_2$), 70.81 ($CH_2$), 70.99 ($CH_2$), 128.23 ($C_6$, CH), 130.09 ($C_6$, CH), 133.23 ($C_6$, C), 145.08 ($C_6$, C−S).

**1,13-Diazido-3,6,9-trioxadecane (2).**[29] Intermediate (**1**) (22.2 g, 0.044 mol) was dissolved in 50 mL of 95% ethanol. Sodium azide (8.5 g, 0.132 mol, 3.0 equiv) dissolved in 25 mL of water was added. The reaction mixture was refluxed under an argon atmosphere for 3 days. The ethanol was removed from the crude reaction mixture by rotary evaporation to leave only the water portion (***Caution!****: do not dry completely for risk of unreacted azide explosion*) which was then extracted with dichloromethane (3 × 250 mL). The organic layer was dried with anhydrous sodium sulfate and the solvent was evaporated to give a light yellow oil (overall yield: 9.30 g, 86%). $^1$H NMR (300 MHz, $CDCl_3$, 25 °C, TMS), $\delta$(ppm) = 3.38 (t, 4H), 3.67 (m, 12H). $^{13}C\{^1H\}$ NMR (500 MHz, $CDCl_3$, 25 °C, TMS) $\delta$(ppm) 50.94 (N−$CH_2$−$CH_2$−O), 70.29 (N−$CH_2$−$CH_2$−O), 70.97 (O−$CH_2$−$CH_2$−O), 70.97 (O−$CH_2$−$CH_2$−O).

**1,13-Diamino-3,6,9-trioxadecane (3).**[29] Lithium aluminum hydride (9.0 g, 0.237 mol) was added under argon atmosphere to 400 mL of freshly distilled tetrahydrofuran (THF) with magnetic stirring. The starting material (**2**) (18.0 g, 0.094 mol) dissolved in 100 mL of THF was then added dropwise over 1 h to the reaction flask on ice. The reaction was refluxed for 24 h before cooling the mixture on an ice bath and quenching excess hydride with slow dropwise addition of 20% NaOH. The resulting white precipitate was filtered away, and the THF was removed by evaporation leaving ∼10 mL of a light yellow aqueous solution. The aqueous solution was extracted with chloroform (3 × 250 mL). The organic layer was collected and dried with anhydrous sodium sulfate before solvent evaporation to give 9.4 g of **3** (52% yield) as a clear oil. $^1$H NMR (500 MHz, $CDCl_3$, 25 °C, TMS) $\delta$ 3.68 (m, 8H), 3.58 (t, 4H), 2.92 (t, 4H) 2.05 (s, $NH_2$). $^{13}C\{^1H\}$ NMR (500 MHz, $CDCl_3$, 25 °C, TMS) $\delta$(ppm) 41.45 (N−$CH_2$−$CH_2$−O), 70.48 ($CH_2$), 70.78 ($CH_2$), 73.53 ($CH_2$).

(18) Bünzli, J.-C. G. *Acc. Chem. Res.* **2006**, *39*, 53–61.
(19) Alexander, V. *Chem. Rev.* **1995**, *95*, 273–342.
(20) Woods, M.; Woessner, D. E.; Zhao, P.; Pasha, A.; Yang, M.-Y.; Huang, C.-H.; Vasalitiy, O.; Morrow, J. R.; Sherry, A. D. *J. Am. Chem. Soc.* **2006**, *128*, 10155–10162.
(21) Woods, M.; Woessner, D. E.; Sherry, A. D. *Chem. Soc. Rev.* **2006**, *35*, 500–511.
(22) Aime, S.; Barge, A.; Castelli, D. D.; Fedeli, F.; Mortillaro, A.; Nielsen, F. U.; Terreno, E. *Magn. Reson. Med.* **2002**, *47*, 639–648.
(23) Ali, M. M.; Woods, M.; Suh, E. H.; Kovacs, Z.; Tircso, G.; Zhao, P.; Kodibagkar, V. D.; Sherry, A. D. *J. Biol. Inorg. Chem.* **2007**, *12*, 855–865.
(24) Yoo, B.; Pagel, M. D. *J. Am. Chem. Soc.* **2006**, *128*, 14032–14033.
(25) Ren, J.; Trokowski, R.; Zhang, S.; Malloy, C. R.; Sherry, A. D. *Magn. Reson. Med.* **2008**, *60*, 1047–1055.
(26) van Zijl, P. C. M.; Jones, C. K.; Ren, J.; Malloy, C. R.; Sherry, A. D. *Proc. Natl. Acad. Sci. U.S.A.* **2007**, *104*, 4359–4364.
(27) Huang, C.-H.; Morrow, J. R. *J. Am. Chem. Soc.* **2009**, *131*, 4206–4207.
(28) Li, A. X.; Wojciechowski, F.; Suchy, M.; Jones, C. K.; Hudson, R. H. E.; Menon, R. S.; Bartha, R. *Magn. Reson. Med.* **2008**, *59*, 374–381.
(29) Gansow, O. A.; Kausar, A. R.; Triplett, K. B. *J. Heterocycl. Chem.* **1981**, *18*, 297–302.

***N*-(*tert*-butyl)-2-bromoacetamide (4).**[30] *t*-Butyl amine (6.65 g, 0.091 mol) was added to 50 mL of dichloromethane. The flask temperature was lowered to −40 °C with a dry ice/acetonitrile bath. Bromoacetyl bromide (9.18 g, 0.050 mol) was added to the reaction dropwise over 45 min, and the reaction was allowed to stir for another 20 min at −40 °C. The resulting white solid (the *t*-butyl amine hydrogen bromide byproduct) was removed by filtration. The solvent was evaporated to give white solid **4** (overall yield: 6.65 g, 69%). $^1$H NMR (300 MHz, $CDCl_3$, 25 °C, TMS), $\delta$(ppm) = 1.38 (s, 9H), 3.79 (s, 2H), 6.27 (s, 1H). $^{13}C\{^1H\}$ NMR (500 MHz, $CDCl_3$, 25 °C, TMS) $\delta$(ppm) 28.66 (q, Br-$CH_2$), 30.15 ($CH_3$), 52.18 ($C(CH_3)_3$), 164.64 (C=O). Mp: 93−95 °C.

**Tetra(*N*-(*tert*-butyl)-acetamide)-1,13-diamino-3,6,9-trioxadecane (L).** Intermediate (**3**) (412 mg, 2.15 mmol) was added to 20 mL of dichloromethane and 1.67 g (12.9 mmol, 6 mol eq.) of diisopropylethylamine (DIPEA). The bromoacetamide (**4**) (2.50 g, 12.9 mmol, 6 mol eq.) was added in one portion and the reaction was refluxed at 45 °C. The reaction progress was monitored with NMR by removing 0.5 mL aliquots of the reaction mixture, drying by rotary evaporation, and dissolving in $CDCl_3$. The total reaction time was typically 4 days. Upon completion of the reaction the mixture was concentrated to a light yellow solid by evaporation. A small amount of toluene (~4 mL) was added, and the solution was stirred for 10 min at room temperature after which it was stored at −20 °C for 10 min to crystallize the DIPEA salt. The salt was filtered away, and the remaining solution was evaporated to a yellow oil. The oil was dissolved into 5 mL of ethyl acetate and loaded on a 2.5 cm diameter × 13 cm long column of 35 mL of neutral alumina using ethyl acetate. The column was washed with 300 mL of ethyl acetate to remove the unreacted bromoacetamide (**4**) from the column. The product which remained at the top of the column was eluted off with 120 mL of 5:1 chloroform/methanol. These fractions were dried with anhydrous sodium sulfate and concentrated by evaporation to give 1.02 g of the final **L** (73% yield) as a light yellow oil. $^1$H NMR (500 MHz, $CDCl_3$, 25 °C, TMS) $\delta$ 1.299 (s, 36H, a and a′ as defined in Scheme 1), 2.695 (t, 4H, d), 3.079 (s, 8H, c and c′), 3.500 (t, 4H, e), 3.570(m, 8H, f, and g), 6.84 (s, 4H, b and b′). $^{13}C\{^1H\}$ NMR (500 MHz, $CDCl_3$, 25 °C, TMS) $\delta$(ppm) 29.06 ($CH_3$), 51.22 ($C(CH_3)_3$), 55.47 (N−$CH_2$−$CH_2$−O), 59.97 (N−$CH_2$−C=O), 68.73 (N−$CH_2$−$CH_2$−O), 70.47 ($CH_2$), 70.86 ($CH_2$), 169.56 (C=O). ESI-MS (*m*/*z*): Found (Calcd.) 645.41 (645.49, **L**-$H^+$).

**Sm(L)$(NO_3)_3$.** Coordination complexes were prepared by dissolving 50 mg (0.075 mmol) of **L** in 2 mL of acetonitrile. Samarium(III) nitrate hexahydrate (0.033 g, 0.075 mmol) was dissolved in 2 mL of acetonitrile. The Sm(III) nitrate solution was added dropwise to the solution of **L** with stirring. After complete addition of Sm(III) solution, the mixture was refluxed for 10 min to obtain a clear colorless solution. Suitable X-ray crystals were obtained after about 2 days by adding 0.2 mL of benzene to a 1 mL portion of the reaction solution. Decomp. point: 305 °C.

**Eu(L)$(NO_3)_3$.** The complex of Eu(III) and **L** was prepared in the same manner as above using ($Eu(NO_3)_3 \cdot 6H_2O$). Suitable X-ray crystals were obtained after about 1 day by adding 0.5 mL of benzene to 1 mL portions of the reaction solution. Decomp. point: 295 °C.

**Yb(L)$(NO_3)_3$.** The complex of Yb(III) and **L** was prepared in the same manner as above using ($Yb(NO_3)_3 \cdot 5H_2O$) and absolute ethanol as the solvent. Suitable X-ray crystals were obtained after about 2 days by adding 0.5 mL of benzene to 1 mL portions of the reaction solution. Decomp. point: 304−306 °C.

**Methods.** NMR spectra were obtained on a Varian Mercury 300 MHz (UMD), Varian 500 MHz (UMD), or Varian 600 MHz (UM) spectrometers at University of Minnesota Duluth (UMD) or the University of Minnesota Twin Cities NMR facilities. The chemical shifts were referenced to the residual solvent signal. One-dimensional proton spectra were recorded using the WEFT pulse sequence which is useful for paramagnetic samples.[31] This pulse sequence uses short pulses and the inversion recovery (180°-$\tau$- 90°), which reduces solvent signals and improves the signal-to-noise of protons near the paramagnetic Ln ion.[32] However, data obtained with normal pulse sequences gave the same results but with more required scans. Paramagnetic chemical exchange saturation transfer (PARACEST) NMR experiments were carried out on a Varian 500 MHz spectrometer. Samples of the Eu(III) complex (75 mM) in water ($H_2O$) were sealed in a melting point capillary tube and placed inside an NMR tube filled with 0.5 mL of $D_2O$. To check for exchangeable protons, spectra were acquired using steady-state irradiation (8 s, 3 dB) on the water resonance. The intensities of the exchangeable −NH protons during $H_2O$ irradiation and without irradiation were compared. UV−visible absorption spectra were recorded on a Shimadzu UV2401 PC UV−visible recording spectrophotometer at room temperature. ESI-MS data on the complexes were obtained at the University of Minnesota Mass Spectrometry Center on a Bruker Biotof II in aqueous 50 mM ammonium acetate, pH 5.1. The capillary exit voltage was 110 V, and the gas temperature was 200 °C. Solution fluorescence spectra and emission decay curves were obtained with a Cary Eclipse Fluorescence Spectrophotometer equipped with a Cary Peltier temperature controller. IR spectra were obtained on KBr pellets of purified powder samples with a Perkin-Elmer Spectrum RX FT-IR spectrophotometer. Isothermal titration calorimetry experiments to determine the binding of Eu(III) to the ligand were performed on a TA Instruments (New Castle, Delaware) Nano ITC at 25 °C. The instrument and its use have previously been described.[33] Both the Eu(III) titrant and the ligand were dissolved in the same buffer consisting of 10 mM MES (99% Sigma) and 100 mM NaCl (Fluka Trace Select) pH 6.0 that was filtered to remove cation impurities with Bio-Rad 100 chelex resin. The calorimetric sample cell was filled with 1.300 mL of solution consisting of 0.5 mM **L**, while the syringe was loaded with 250 $\mu$L of 4 mM $Eu(NO_3)_3$. The reference cell was filled with Milli-Q water. The stir speed was 250 rpm, and the interval between injections was 300 s. Eu(III) was added in a 1 $\mu$L injection to displace air from the syringe followed by 49 × 5 $\mu$L injections. The raw heats were integrated, and the heat of dilution was subtracted by injecting 4 mM $Eu(NO_3)_3$ into 10 mM MES, 100 mM NaCl buffer. The subtracted heats were then fit using the independent binding model (single site) from TA Instruments Bindworks software.

**X-ray Analysis.** Single-crystal determination for the Yb(III) complex was carried out using a Bruker SMART Apex II diffractometer at 100 K using graphite-monochromated Cu K$\alpha$ radiation.[34] The data was corrected for Lorentz and polarization[35] effects and absorption using SADABS.[36] The structure was solved by use of Patterson mapping. Least squares refinement on $F^2$ was used for all reflections. Structure solution, refinement, and the calculation of derived results was performed using the SHELXTL[37] software package. The non-hydrogen atoms were refined anisotropically. The hydrogen atoms were located and then placed in theoretical positions. Images of molecular structures were created using Ortep III[38]

X-ray diffraction data for the Eu(III) and Sm(III) complexes were collected with a Rigaku AFC-7R diffractometer

(30) Pospisil, J.; Travnicek, M.; Potacek, M. *ARKIVOC* **2001**, 146–162.

(31) Kalverda, A. P.; Salgado, J.; Dennison, C.; Canters, G. W. *Biochemistry* **1996**, *35*, 3085–3092.

(32) Inubushi, T.; Becker, E. D. *Magn. Reson.* **1983**, *51*, 128–133.

(33) Wiseman, T.; Williston, S.; Brandts, J. F.; Lin, L. N. *Anal. Biochem.* **1989**, *179*, 131–137.

(34) *Smart, Apex ii, Data Collection Software*, Version 2.1; Bruker AXS Inc.: Madison, WI, 2005.

(35) *Saint Plus*, D. R. S., Version 7.34a; Bruker AXS Inc.: Madison, WI, 2005.

(36) Sheldrick, G. M. *SADABS*; University of Göttingen: Göttingen, Germany, 2005.

(37) Sheldrick, G. M. *Acta Crystallogr*., Sect. A A64, **2008**.

(38) Farrugia, L. J. *J. Appl. Crystallogr*. **1997**, 30.

**Scheme 2.** Reagents and Conditions[a]

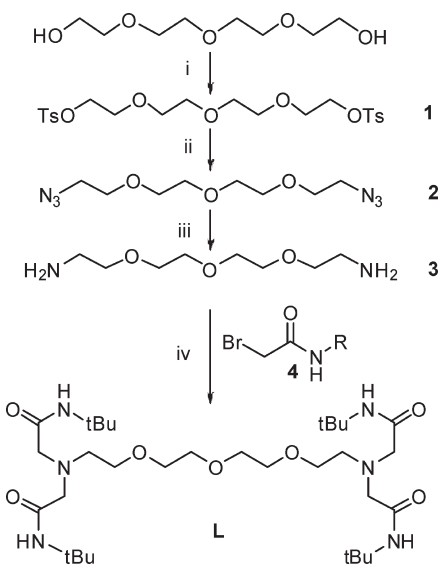


[a] (i.) TsCl, Pyridine, −20 °C, 4 h (76%); (ii.) $NaN_3$, 95% EtOH, reflux 3 days (86%); (iii.) $LiAlH_4$, THF, reflux 1 day (52%); (iv.) Br-*t*-butylamide (**4**), DIPEA, DCM, reflux, 4 days (78%).

at 298 K using graphite-monochromated Mo Kα radiation ($\lambda$ = 0.71073 Å). $\psi$-Scan absorption corrections were applied to the data by using the TeXsan 10.3b program (Rigaku Inc. 1997). The structure was solved by use of Patterson map and refined by full-matrix least-squares refinement on $F^2$ with the Crystals for Windows program.

All H atoms were positioned geometrically except for the −NH hydrogen atoms which were located on the Fourier map. The Eu(III) positional disorder was modeled in carbon atoms 3, 4, and 5. Disorder in the tertiary butyl groups and nitrate ions were not modeled. The structures of the Sm(III) and Yb(III) complexes have similar disorder in the ligand backbone $CH_2$ atoms as seen in the Eu(III) structure which was not modeled.

## Results and Discussion

**Synthesis and Characterization of L.** There are multiple examples of amide ligands coordinated to transition metal ions, such as Ni(II), Zn(II), and Cu(II).[39,40] The coordination of a large chain chelating ligand to lanthanide ions using substituted amide groups has fewer examples.[41] To assemble a stable lanthanide complex with amide groups we designed a ligand that had several oxygen donor atoms available for bonding. Large chelating multidentate ligands with hard donor atoms are preferred for stable complex formation.[19] Large ligands with multiple donating atoms have the added benefit of blocking solvent coordination and entropically favoring complex formation.[18] The synthesis scheme for the ligand **L** (Scheme 2) follows several known procedures[29,30,42] with easily modified conditions to generate varied amide R groups through the use of different bromoamides (**4** in Scheme 2).[30] This enables the ligand to be tuned to achieve different structures and complex properties. For example, attaching a strongly absorbing aromatic ligand could help increase the luminescence of the Ln complexes.[43] Also, different bulky R groups could be used to alter the coordination geometry. We report the synthesis of the *t*-butyl containing ligand, **L**.

The steps used to synthesize **L** were routine. Step (iv.) of the synthesis (Scheme 2), however, required some tuning. Several solvents were attempted in this step which involves adding the bromoacetamide to the diamine backbone of the ligand. It was found that the lower refluxing dichloromethane favored the formation of the desired tetra-substituted ligand whereas the higher refluxing toluene and acetonitrile resulted in quaternary ammonium side products, with a total of 5 or 6 amide group substitutions. The choice of the base used in this step was also significant, with bulkier amine bases being preferred. The reaction was attempted using triethylamine but it was found that the reaction between the bromoacetamide and triethylamine formed a significant side product. The use of diisopropylethylamine (DIPEA) did not show any side reaction with the bromoacetamide. Only the DIPEA bromide salt was formed as expected which was easily removed from the reaction solution by precipitation with toluene.

**X-ray Structures.** Colorless X-ray quality crystals were grown over several days from 19 mM solutions in acetonitrile of 1:1 ligand:Ln(III) nitrate with the addition of benzene (the Yb(III) complex was grown from absolute ethanol/benzene). The crystals appeared clear in solution but slowly turned opaque once removed from solvent indicating loss of solvent molecules from the crystal lattice. All three of the Ln(III) complexes crystallized in the monoclinic crystal system but in different space groups (Table 1). In the three metal complexes the ligand completely wrapped around the Ln(III) ion and coordinated through all four of the amide carbonyl oxygens, all three of the ether oxygens, and the two tertiary nitrogens. Coordination was seen through the amide carbonyl oxygen instead of the nitrogen as commonly found with other similar complexes. All of the complexes show some amount of disorder in the *t*-butyl groups as well as the nitrate anions. No attempt was made to model this disorder since it was not relevant to the analysis of the structures. There was, however, disorder present in some of the ether backbone carbons in the Sm(III) and Eu(III) structures. This disorder was modeled in the Eu(III) complex since its spectroscopy is the focus of this paper.

**[SmL]$^{3+}$ Crystal Structure.** The X-ray diffraction data indicates the Sm**L**$(NO_3)_3$ complex (Figure 1) crystallizes as a mononuclear species and forms a nine coordinate complex with a tricapped trigonal prismatic structure. The Sm(III) complex was grown from a solution with an acetonitrile and benzene solvent system, both of which are found in the crystal structure. The complex crystallizes with one molecule of acetonitrile and benzene as well as three nitrate counterions. There is a small area of electron density found on the Fourier map that is not very well-defined and was modeled as a water molecule. The nitrate anions and *t*-butyl groups were disordered as well as the carbon atoms in the ether backbone of the ligand. The complex possesses a pseudo 2-fold rotation

(39) Teo, S.-B.; Ng, C.-H.; Teoh, S.-G.; Wei, C. *Polyhedron* **1994**, *13*, 2537–2542.
(40) Ng, C. H.; Lin, C. M.; Chang, T. M.; Teoh, S. G.; Yap, S. Y.; Ng, S. W. *Polyhedron* **2006**, *25*, 1287–1291.
(41) Lei, K.-W.; Liu, W.-S.; Tan, M.-Y. *Spectrochim. Acta, Part A* **2007**, *66A*, 118–125.
(42) Moore, J. L.; Taylor, S. M.; Soloshonok, V. A. *ARKIVOC* **2005**, 287–292.
(43) Parker, D.; Dickins, R. S.; Puschmann, H.; Crossland, C.; Howard, J. A. K. *Chem. Rev.* **2002**, *102*, 1977–2010.

**Table 1.** Crystal Data, Collection and Structure Refinement Parameters for Complexes $[SmL]^{3+}$, $[EuL]^{3+}$, and $[YbL]^{3+}$

| | $Sm\cdot L\cdot(NO_3)_3\cdot H_2O\cdot C_6H_6\cdot CH_3CN$ | $Eu\cdot L\cdot(NO_3)_3\cdot CH_3CN$ | $Yb\cdot L\cdot(NO_3)_3\cdot C_2H_6O$ |
|---|---|---|---|
| empirical formula | $C_{40}H_{75}N_{10}O_{17}Sm$ | $C_{34}H_{67}N_{10}O_{16}Eu$ | $C_{34}H_{70}N_9O_{17}Yb$ |
| formula weight | 1118.44 | 1023.92 | 1050.03 |
| crystal System | monoclinic | monoclinic | monoclinic |
| space group | $P2_1/c$ | $P2_1/n$ | $C2/c$ |
| crystal size ($mm^3$) | $0.30 \times 0.30 \times 0.60$ | $0.50 \times 0.30 \times 0.30$ | $0.44 \times 0.26 \times 0.24$ |
| temperature (K) | 298(2) | 298(2) | 100(2) |
| $a$(Å) | 21.198(4) | 13.010(3) | 34.436(5) |
| $b$(Å) | 16.070(3) | 17.667(4) | 14.172(18) |
| $c$(Å) | 16.119(3) | 20.897(4) | 20.786(3) |
| $\beta$(deg) | 102.39(3) | 98.12(3) | 96.331(6) |
| V(Å$^3$) | 5363.1(18) | 4755.0(17) | 10082.0(2) |
| Z | 4 | 4 | 8 |
| $\rho_{calc}$(g cm$^{-3}$) | 1.385 | 1.430 | 1.384 |
| $\mu$(mm$^{-1}$) | 1.168 | 1.392 | 4.033 |
| $F_{000}$ | 2332 | 2128 | 4344 |
| $R_1\{I > 2\sigma(I)\}$ | 0.0617 | 0.0558 | 0.0385 |
| $wR_2\{I > 2\sigma(I)\}$ | 0.1319 | 0.1468 | 0.1102 |
| $R_1$ (all data) | 0.1139 | 0.0702 | 0.0402 |
| $wR_2$ (all data) | 0.1530 | 0.1554 | 0.1117 |
| goodness-of-fit | 0.900 | 1.014 | 1.081 |

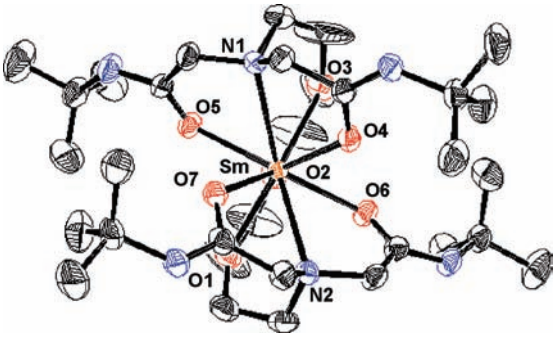


**Figure 1.** X-ray crystal structure of the $[SmL]^{3+}$ complex at a 30% probability level. The structure is shown without solvent molecules or counterion molecules for clarity. An axis through Sm and O2 is the location of the pseudo-$C_2$ axis.

axis (Figure 1) passing through the Sm(III) ion and the central ether oxygen (O2) atom. This suggests that half of the molecule is approximately equivalent to the other half divided down the O2 atom.

The average Sm−O amide carbonyl and Sm−O ether distances are 2.37 and 2.51 Å, respectively (Table 2 and 3). The average bond lengths found in other similar Sm(III) complexes are 2.38 and 2.58 Å, respectively (the range of bond distances are 2.37−2.38 Å and 2.50−2.73 Å, respectively).[44−52] This indicates that the Sm(III) complex has a typical carbonyl amide to Sm(III) distance. However, the ether to Sm(III) distance is on the short end of what is typically observed. A majority of the Sm(III) complexes containing a bonded ether group (excluding solvent molecules such as THF) are formed using crown ethers, where the Sm(III) to ether distance is dictated somewhat by the rigidity of the crown. The ligand **L** has 4 chelating side chains that might pull the ether oxygens closer to the Sm(III) than expected in the crown cases. The average Sm−N distance is 2.67 Å and is slightly shorter than the average Sm−N bond distance of 2.69 Å seen in other complexes (which range 2.560−2.818 Å).[45,53−59]

**Table 2.** Selected Bond Lengths (Å) for $[SmL]^{3+}$, $[EuL]^{3+}$, and $[YbL]^{3+}$

| | | | | | |
|---|---|---|---|---|---|
| Sm1−O1 | 2.493(5) | Eu1−O1 | 2.488(4) | Yb1−O1 | 2.409(4) |
| Sm1−O2 | 2.532(5) | Eu1−O2 | 2.516(4) | Yb1−O2 | 2.445(4) |
| Sm1−O3 | 2.518(6) | Eu1−O3 | 2.473(4) | Yb1−O3 | 2.401(4) |
| Sm1−O4 | 2.398(5) | Eu1−O4 | 2.358(4) | Yb1−O4 | 2.299(4) |
| Sm1−O5 | 2.379(5) | Eu1−O5 | 2.399(3) | Yb1−O5 | 2.282(4) |
| Sm1−O6 | 2.375(5) | Eu1−O6 | 2.374(4) | Yb1−O6 | 2.305(4) |
| Sm1−O7 | 2.337(5) | Eu1−O7 | 2.346(4) | Yb1−O7 | 2.293(4) |
| Sm1−N1 | 2.686(6) | Eu1−N1 | 2.658(5) | Yb1−N1 | 2.613(5) |
| Sm1−N2 | 2.647(6) | Eu1−N2 | 2.625(4) | Yb1−N2 | 2.581(5) |

**Table 3.** Average Ln−O, Ln−N Bond Lengths (Å) for Complexes $[SmL]^{3+}$, $[EuL]^{3+}$, and $[YbL]^{3+}$

| $[SmL]^{3+}$ | | $[EuL]^{3+}$ | | $[YbL]^{3+}$ | |
|---|---|---|---|---|---|
| **Sm−O** | | **Eu−O** | | **Yb−O** | |
| ether oxygens | 2.51 | | 2.49 | | 2.42 |
| Carbonyl oxygens | 2.37 | | 2.37 | | 2.29 |
| **Sm−N** | 2.67 | **Eu−N** | 2.64 | **Yb−N** | 2.60 |

(44) Rogers, R. D.; Rollins, A. N.; Etzenhouser, R. D.; Voss, E. J.; Bauer, C. B. *Inorg. Chem.* **1993**, *32*, 3451–3462.
(45) Schumann, H.; Rosenthal, E. C. E.; Demtschuk, J.; Molander, G. A. *Organometallics* **1998**, *17*, 5324–5333.
(46) Grob, T.; Harms, K.; Dehnicke, K. *Z. Anorg. Allg. Chem.* **2001**, *627*, 125–127.
(47) Evans, W. J.; Giarikos, D. G.; Johnston, M. A.; Greci, M. A.; Ziller, J. W. *J. Chem. Soc., Dalton Trans.* **2002**, 520–526.
(48) Vestergren, M.; Gustafsson, B.; Johansson, A.; Hakansson, M. *J. Organomet. Chem.* **2004**, *689*, 1723–1733.
(49) Sen, A.; Chebolu, V.; Rheingold, A. L. *Inorg. Chem.* **1987**, *26*, 1821–1823.
(50) Parker, D.; Puschmann, H.; Batsanov, A. S.; Senanayake, K. *Inorg. Chem.* **2003**, *42*, 8646–8651.
(51) Bretonniere, Y.; Wietzke, R.; Lebrun, C.; Mazzanti, M.; Pecaut, J. *Inorg. Chem.* **2000**, *39*, 3499–3505.
(52) Batsanov, A. S.; Bruce, J. I.; Ganesh, T.; Low, P. J.; Kataky, R.; Puschmann, H.; Steel, P. G. *J. Chem. Soc., Perkin Trans.* **2002**, 932–937.
(53) Bonnet, F.; Hillier, A. C.; Collins, A.; Dubberley, S. R.; Mountford, P. *Dalton. Trans.* **2005**, 421–423.
(54) Blake, A. J.; Doble, D. M. J.; Li, W.-S.; Schroder, M. *J. Chem. Soc., Dalton Trans.* **1997**, 3655–3657.
(55) Kang, J.-G.; Kang, H.-J.; Jung, J.-S.; Yun, S. S.; Kim, C.-H. *Bull. Korean Chem. Soc.* **2004**, *25*, 852–858.
(56) Torres, J.; Kremer, C.; Kremer, E.; Dominguez, S.; Mederos, A.; Arrieta, J. M. *Inorg. Chim. Acta* **2003**, *355*, 175–182.
(57) Giesbrecht, G. R.; Cui, C.; Shafir, A.; Schmidt, J. A. R.; Arnold, J. *Organometallics* **2002**, *21*, 3841–3844.
(58) Mizukami, S.; Houjou, H.; Kanesato, M.; Hiratani, K. *Chem.—Eur. J.* **2003**, *9*, 1521–1528.
(59) Essig, M. W.; Webster Keogh, D.; Scott, B. L.; Watkin, J. G. *Polyhedron* **2001**, *20*, 373–377.

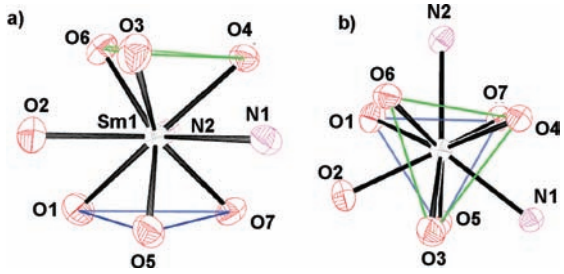


**Figure 2.** Coordination polyhedron of the Sm(III) complex.

**Table 4.** Angles Defining the Polyhedron Based on the Method of Guggenberger and Muetterties[60]

| | average angle (degrees) | | | |
|---|---|---|---|---|
| faces | $[SmL]^{3+}$ | $[EuL]^{3+}$ | $[YbL]^{3+}$ | ideal $D_{3h}$ |
| opposed (⊥) | 176.69 | 177.15 | 175.24 | 180.00 |
| opposed (∥) | 143.81 | 142.90 | 141.32 | 146.40 |
| vicinal (∥) | 23.97 | 23.04 | 21.39 | 26.40 |

The C−N bond of the amide group in the complex was shortened to 1.310 Å compared to the amide C−N distance in typical organic molecules of 1.334 Å. This indicates more double bond character which would increase the acidity of the −NH bond. This acidic character was supported by the addition of $D_2O$ in NMR experiments as well as the mass spectrometry experiments (see Supporting Information). A survey of several C−N bond distances in other Sm(III) complexes containing amide functional groups yielded average bond distances ranging from 1.308 to 1.321 Å showing that the $[SmL]^{3+}$ complex has amide C−N distances on the shorter side.[50−52]

The Sm(III) complex polyhedron (Figure 2) was analyzed using method of Guggenberger and Muetterties.[60] A summary of these results are shown in Table 4. The geometry of the polyhedron can be best described as a tricapped trigonal prism with distorted $D_{3h}$ symmetry. There is a deviation of 3.31 degrees between the top and bottom triangular faces (Figure 2a).

**$[EuL]^{3+}$ Crystal Structure.** The X-ray structure of the $EuL(NO_3)_3$ complex (Figure 3) is similar to that of the Sm(III) structure. The complex crystallizes with three nitrate counterions and one acetonitrile solvent molecule. The nitrate anions and *t*-butyl groups were disordered as well as the carbon atoms in the ether backbone of the ligand. The most disordered atoms in the ligand backbone, C2, C3, and C5, were modeled and fit with the atoms occupying two different positions. The structure of the Eu(III) complex has the same type of pseudo $C_2$ symmetry as seen in the Sm(III) complex.

The average Eu−O amide carbonyl and Eu−O ether distances in $[EuL]^{3+}$ are 2.37 and 2.49 Å, respectively (Table 2 and 3). These average bond lengths found in other similar Eu(III) complexes are 2.377 and 2.568 Å, respectively (bond distances range from 2.268 to 2.415 Å and 2.460−2.697 Å, respectively).[50,52,61−71] This indicates that the Eu(III) complex has a typical carbonyl amide to Eu(III) distance. However, the ether to Eu(III) distance is slightly shorter than what is typically observed. The average Eu−N bond distance was found to be 2.64 Å which is slightly shorter than the average bond distance of 2.67 Å found in similar complexes (bond distances range from 2.513 to 2.760 Å).[55,61,68,72−79]

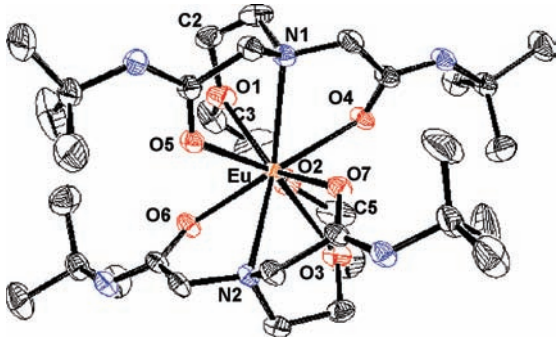


**Figure 3.** X-ray crystal structure of the $[EuL]^{3+}$ complex at a 30% level. The structure is shown without solvent or counterions for clarity.

The C−N bond of the amide group in the complex appeared shortened to 1.299 Å compared to the amide C−N distance in regular organic molecules. The acidic character of the resulting −NH group was supported by NMR experiments and mass spectra (see below). Importantly, the readily exchangeable protons make the chemical exchange saturation transfer (CEST) NMR experiments possible (see below). A survey of several C−N bond distances in other Eu(III) complexes containing amide functional groups gave average bond distances ranging from 1.307 to 1.332 Å showing that our Eu(III) complex is on the shorter side of typical amide C−N distances.[50,52,64−71]

(60) Guggenberger, L. J.; Muetterties, E. L. *J. Am. Chem. Soc.* **1976**, *98*, 7221–7225.
(61) Saleh, M. I.; Salhin, A.; Saad, B.; Fun, H.-K. *J. Mol. Struct.* **1999**, *475*, 93–103.
(62) Zhang, K.; Zhang, W.; Wang, S.; Sheng, E.; Yang, G.; Xie, M.; Zhou, S.; Feng, Y.; Mao, L.; Huang, Z. *Dalton. Trans.* **2004**, 1029–1037.
(63) Bünzli, J. C. G.; Leonard, G. A.; Plancherel, D.; Chapuis, G. *Helv. Chim. Acta* **1986**, *69*, 288–297.
(64) Jiang, W.; Liu, W.; Li, X.; Wen, Y.; Tan, M.; Yu, K. *J. Mol. Struct.* **2002**, *611*, 33–37.
(65) Binyamin, I.; Pailloux, S.; Duesler, E. N.; Rapko, B. M.; Paine, R. T. *Inorg. Chem.* **2006**, *45*, 5886–5892.
(66) Gunnlaugsson, T.; Davies, R. J. H.; Nieuwenhuyzen, M.; Stevenson, C. S.; Viguier, R.; Mulready, S. *Chem. Commun.* **2002**, 2136–2137.
(67) Gunnlaugsson, T.; Leonard, J. P.; Mulready, S.; Nieuwenhuyzen, M. *Tetrahedron* **2004**, *60*, 105–113.
(68) Zucchi, G.; Scopelliti, R.; Bünzli, J.-C. G. *J. Chem. Soc., Dalton Trans.* **2001**, 1975–1985.
(69) Gunnlaugsson, T.; Davies, R. J. H.; Kruger, P. E.; Jensen, P.; McCabe, T.; Mulready, S.; O'Brien, J. E.; Stevenson, C. S.; Fanning, A.-M. *Tetrahedron Lett.* **2005**, *46*, 3761–3766.
(70) Aime, S.; Barge, A.; Botta, M.; Howard, J. A. K.; Kataky, R.; Lowe, M. P.; Moloney, J. M.; Parker, D.; de Sousa, A. S. *Chem. Commun.* **1999**, 1047–1048.
(71) Dickins, R. S.; Howard, J. A. K.; Lehmann, C. W.; Moloney, J.; Parker, D.; Peacock, R. D. *Angew. Chem., Int. Ed. Engl.* **1997**, *36*, 521–523.
(72) Nicolo, F.; Plancherel, D.; Chapuis, G.; Bünzli, J. C. G. *Inorg. Chem.* **1988**, *27*, 3518–3526.
(73) Janicki, R.; Mondry, A.; Starynowicz, P. *Polyhedron* **2007**, *26*, 845–850.
(74) Chen, Q.-Y.; Luo, Q.-H.; Hu, X.-L.; Shen, M.-C.; Chen, J.-T. *Chem.—Eur. J.* **2002**, *8*, 3984–3990.
(75) Mondry, A.; Janicki, R. *Dalton. Trans.* **2006**, 4702–4710.
(76) Howard, J. A. K.; Kenwright, A. M.; Moloney, J. M.; Parker, D.; Woods, M.; Port, M.; Navet, M.; Rousseau, O. *Chem. Commun.* **1998**, 1381–1382.
(77) Quici, S.; Marzanni, G.; Forni, A.; Accorsi, G.; Barigelletti, F. *Inorg. Chem.* **2004**, *43*, 1294–1301.
(78) Platas, C.; Avecilla, F.; de Blas, A.; Geraldes, C. F. G. C.; Rodriguez-Blas, T.; Adams, H.; Mahia, J. *Inorg. Chem.* **1999**, *38*, 3190–3199.
(79) Wietzke, R.; Mazzanti, M.; Latour, J. M.; Pecaut, J. *Chem. Commun.* **1999**, 209–210.

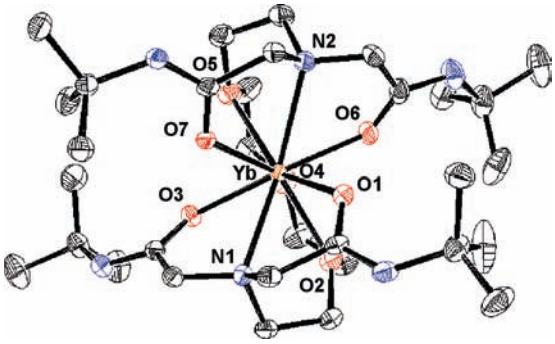


**Figure 4.** X-ray crystal structure of the $[YbL]^{3+}$ complex at a 40% probability level. The structure is shown without counterion molecules for clarity.

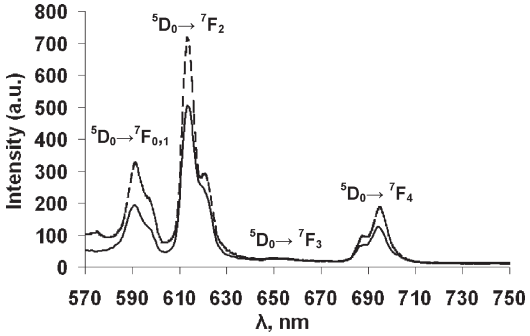


**Figure 5.** Emission spectra of $[EuL]^{3+}$ crystals (dashed line) and solution (solid line) shown at 3× intensity. ($\lambda_{ex}$ = 397 nm, 19 mM solution in acetonitrile, 22 °C).

The shape of the coordination polyhedron is a distorted tricapped trigonal prism according to the method of Guggenberger and Muetterties (Table 4).[60] There is a distortion between the top and bottom triangular faces of 2.85 degrees. This is slightly smaller than the deviation seen in the Sm(III) structure and could be attributed to different crystal packing forces or the slightly smaller size of the Eu(III) ion relative to that of the Sm(III) ion. Indeed, the average bond distances are generally slightly shorter in the Eu(III) complex than in the Sm(III) complex reflecting the decrease in ionic radius in moving across the f-block series.

**$[YbL]^{3+}$ Crystal Structure.** The X-ray crystal structure of the $YbL(NO_3)_3$ complex is similar to the Eu(III) and Sm(III) structures (Figure 4). The Yb(III) complex was grown from a solution with an absolute ethanol and benzene solvent system. The complex crystallizes with three nitrate counterions and one ethanol molecule. The Yb(III) complex shows the same pseudo $C_2$ symmetry as seen in the Eu(III) and Sm(III) structures.

The average Yb−O amide carbonyl and Yb−O ether distances are 2.29 and 2.42 Å, respectively (Table 3). The average bond lengths found in other similar Yb(III) complexes are 2.29 and 2.46 Å, respectively (the range of bond distances are 2.218−2.313 Å and 2.359−2.554 Å, respectively).[48,62,80−92] The average Yb−N distance is 2.60 Å and is longer than the average Yb−N bond distance of 2.57 Å seen in other complexes (which range 2.503−2.713 Å).[87,92−99]

As seen in the Eu(III) and Sm(III) complexes, the amide C−N bond has also been shortened to 1.324 Å relative to a typical organic molecule amide. Addition of $D_2O$ in NMR experiments confirms the presence of acidic exchangeable protons. The Yb(III) complex polyhedron was also analyzed using the method of Guggenberger and Muetterties (Table 4).[60] There is a deviation of 4.76 degrees between the top and bottom triangular faces of the tricapped trigonal prism. This is the largest deviation seen in the three complexes studied. The Yb(III) ion is the smallest of the lanthanide series. Indeed, the average bond distances in the Yb(III) complex are significantly shorter than the other complexes, reflecting the decrease in ionic radius moving across the f-block.

**Absorbance and Luminescence Spectroscopy.** The Eu(III) fluorescence is normally preceded by ligand to metal energy transfer following ligand absorption.[100] Ligand **L** lacks strongly absorbing aromatic groups leading to inefficient absorption and also possibly poor energy transfer to the metal. The solution ligand absorbance (data not shown) is relatively featureless except for a weak absorbance around 220 nm, which likely arises from the amide functionality. The absorbance of the $[EuL]^{3+}$ complex in solution is nearly identical but with about 2-fold increase in intensity. Direct excitation into the ligand was attempted with wavelengths from 200 to 329 nm, where little to no emission intensity was observed.

Because of the inefficient absorption by the ligand, we chose excitation at 397 nm which directly excites the metal centered $^7F_0$ to $^5L_6$ transition (Figure 5).[101] This is a

(80) Xu, X.; Hu, M.; Yao, Y.; Qi, R.; Zhang, Y.; Shen, Q. *J. Mol. Struct.* **2007**, *829*, 189–194.
(81) Deacon, G. B.; Fanwick, P. E.; Gitlits, A.; Rothwell, I. P.; Skelton, B. W.; White, A. H. *Eur. J. Inorg. Chem.* **2001**, 1505–1514.
(82) Wong, W.-K.; Zhang, L.; Xue, F.; Mak, T. C. W. *J. Chem. Soc., Dalton Trans.* **1999**, 3053–3062.
(83) Qian, C.; Zou, G.; Jiang, W.; Chen, Y.; Sun, J.; Li, N. *Organometallics* **2004**, *23*, 4980–4986.
(84) Deacon, G. B.; MacKinnon, P. I.; Hambley, T. W.; Taylor, J. C. *J. Organomet. Chem.* **1983**, *259*, 91–97.
(85) Pi, C.; Zhang, Z.; Liu, R.; Weng, L.; Chen, Z.; Zhou, X. *Organometallics* **2006**, *25*, 5165–5172.
(86) Steudel, A.; Stehr, J.; Siebel, E.; Fischer, R. D. *J. Organomet. Chem.* **1998**, *570*, 89–96.
(87) Benetollo, F.; Bombieri, G.; Depaoli, G.; Truter, M. R. *Inorg. Chim. Acta* **1996**, *245*, 223–229.
(88) Wang, S.; Li, H.-W.; Xie, Z. *Organometallics* **2004**, *23*, 2469–2478.
(89) Gun'ko, Y. K.; Hitchcock, P. B. *Chem. Commun.* **1998**, 1843–1844.
(90) Batsanov, A. S.; Beeby, A.; Bruce, J. I.; Howard, J. A. K.; Kenwright, A. M.; Parker, D. *Chem. Commun.* **1999**, 1011–1012.
(91) Dickins, R. S.; Aime, S.; Batsanov, A. S.; Beeby, A.; Botta, M.; Bruce, J. I.; Howard, J. A. K.; Love, C. S.; Parker, D.; Peacock, R. D.; Puschmann, H. *J. Am. Chem. Soc.* **2002**, *124*, 12697–12705.
(92) Vipond, J.; Woods, M.; Zhao, P.; Tircso, G.; Ren, J.; Bott, S. G.; Ogrin, D.; Kiefer, G. E.; Kovacs, Z.; Sherry, A. D. *Inorg. Chem.* **2007**, *46*, 2584–2595.
(93) Monteiro, B.; Roitershtein, D.; Ferreira, H.; Ascenso, J. R.; Martins, A. M.; Domingos, A.; Marques, N. *Inorg. Chem.* **2003**, *42*, 4223–4231.
(94) Neculai, A. M.; Neculai, D.; Roesky, H. W.; Magull, J. *Polyhedron* **2004**, *23*, 183–187.
(95) Bochkarev, M. N.; Fedushkin, I. L.; Nevodchikov, V. I. Protchenko, A. V.; Schumann, H.; Girgsdies, F. *Inorg. Chim. Acta* **1998**, *280*, 138–142.
(96) Smith, P. H.; Raymond, K. N. *Inorg. Chem.* **1985**, *24*, 3469–3477.
(97) Qian, C.; Li, H.; Sun, J.; Nie, W. *J. Organomet. Chem.* **1999**, *585*, 59–62.
(98) Bernhardt, P. V.; Flanagan, B. M.; Riley, M. J. *Aust. J. Chem.* **2001**, *54*, 229–232.
(99) Herbrich, T.; Thiele, K.-H.; Thewalt, U. *Z. Anorg. Allg. Chem.* **1996**, *622*, 1609–1611.
(100) Werts, M. H. V. *Sci. Prog.* **2005**, *88*, 101–131.
(101) Kumar, A.; Rai, D. K.; Rai, S. B. *Spectrochim. Acta, Part A* **2002**, *58A*, 2115–2125.

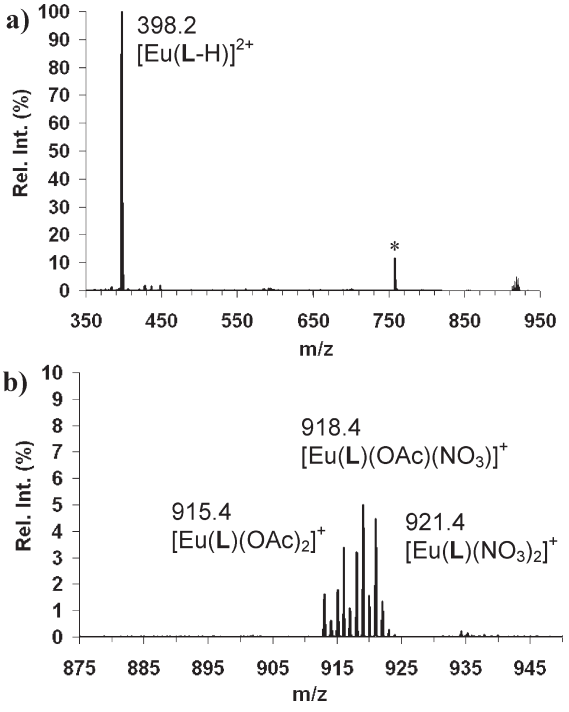


**Figure 6.** ESI mass spectrum of the Eu(III) complex. (a) Full spectrum. The trace penta-substituted ligand impurity is denoted by *. (b) Close-up view showing the peak around 920 *m*/*z*.

common method for the observation of Eu(III) fluorescence when the ligand has inefficient energy transfer to the metal.[102,103] Figure 5 shows a comparison between the emission of crystals and solution of the Eu(III) complex. The peak positions and general shape are similar for both solution and solid state emission at both wavelengths, and they are completely different from that of $Eu(NO_3)_3$ (not shown). This is consistent with the complex having similar solution and solid state structures.

The emission spectrum for $[Eu\mathbf{L}]^{3+}$ (Figure 5) shows transitions from $^5D_0$ to the $^7F_0$, $^7F_1$, $^7F_2$, and $^7F_3$, and $^7F_4$ states observed around 580, 590, 615, 650, and 690 nm, respectively.[100] The splitting of the $^7F_1$, $^7F_2$, $^7F_3$, and $^7F_4$ states into their stark components suggests that the complex has low symmetry.[104]

**Mass Spectroscopy.** The ESI mass spectrum of the Eu(III) complex is shown in Figure 6. The spectrum shows three overlapping species around 920 *m*/*z* corresponding to $[Eu\mathbf{L}(OAc)_2]^+$, $[Eu\mathbf{L}(OAc)(NO_3)]^+$, and $[Eu\mathbf{L}(NO_3)_2]^+$, at 915.4, 918.4, and 921.4 *m*/*z*, respectively (Figure 6b) (masses are for the most abundant isotope of Eu). There is the major peak at 398.2 *m*/*z* that is assigned to the doubly charged $[Eu(\mathbf{L}\text{-}2H)]^{2+}$ ion, where L lost two protons. This is consistent with the acidic nature of the −NH protons, as supported by the X-ray and NMR data, wherein the amide C−N bond is shorter and the −NH protons are readily exchanged with $D_2O$. The presence of these species in the mass spectrum provides evidence that there is a mononuclear form of the complex present in solution. Similar results were obtained for the Sm(III) and Yb(III) complexes (see Supporting Information). The spectrum

**Table 5.** IR Spectra Data of the Free Ligands and Their Complexes ($cm^{-1}$)

| | $\nu$(C=O) | $\nu$(C−O−C) | $\nu$(free $NO_3^-$) |
|---|---|---|---|
| **L** | 1655 | 1227 | |
| $[Eu\mathbf{L}]^{3+}$ | 1618 | 1216 | 1384 |
| $[Sm\mathbf{L}]^{3+}$ | 1617 | 1214 | 1384 |
| $[Yb\mathbf{L}]^{3+}$ | 1617 | 1219 | 1383 |

(Figure 6a) also shows a peak at 758.4 *m*/*z* that is consistent with a trace amount of penta-substituted **L** (ligand with 5 amide arms) that shows up strongly in ESI-MS.

**IR Spectroscopy.** The IR spectrum of the free ligand shows bands at 1655 and 1227 $cm^{-1}$ which are assigned to the amide carbonyl and backbone ether atoms, respectively. The coordination of a large Ln(III) ion to an organic ligand would be expected to lower the IR vibrational frequencies of groups coordinated directly to the lanthanide. This is likely a result of the ionic Ln(III) ion polarizing electron density in the group and decreasing the bond order. A summary of the groups directly bonded to the Ln(III) ions is shown in Table 5. In the Ln(III) complexes these bands are shifted to lower frequencies as expected. There is also a strong band at 1384 in all of the Ln(III) complexes. This band can be assigned to the free nitrate ion. There is an absence of bands around 1493, 1311, and 816 $cm^{-1}$ which are indicative of Ln(III)-nitrate bound species.[41] The presence of free nitrate and absence of any Ln(III) bonded nitrate is in agreement with the crystallography results.

**Binding Studies Using ITC.** To determine the solution stability the Eu(III)**L** complex, experiments using isothermal titration calorimetry (ITC) were performed. Binding constants can be derived from experiments monitoring changes in the UV−vis absorption spectrum[105,106] or with pH potentiometric titrations.[107] Alternatively, ITC directly measures the heat released or absorbed during the binding event and allows accurate determination of binding constants. ITC of Eu(III) and **L** show that the Eu(III) ion binds to the ligand with a binding constant of 9.5 (log *K*) (see Supporting Information). For comparison, the binding constants with other lanthanide ligands, such as the popular MRI ligand DOTA and EDTA, are about 23.5 and 17.4 (log *K*), respectively as determined by potentiometry.[108,109] Complexes of tetra amide derivatives of DOTA give lower log *K* constants of about 13.80.[107] The neutrally charged amide containing ligands do not have as high binding affinities as comparable ligands containing anionic carboxylic acid groups.

**NMR Spectroscopy.** The NMR spectra of the Ln(III) complexes were investigated to determine the complexes' structure in solution. Complexes were prepared *in situ* by mixing equal molar amounts of ligand and Ln(III) nitrate in $CD_3CN$. $^1H$ NMR spectra of paramagnetic Ln(III)**L** complexes (Ln = Sm, Eu, and Yb) were obtained in $CD_3CN-D_2O$ solutions (Figure 7). Samples were run in both $CD_3CN$ and $CD_3CN-D_2O$, and it was found that the

(102) Lucas, R. L.; Benjamin, M.; Reineke, T. M. *Bioconjugate Chem.* **2008**, *19*, 24–27.
(103) Zhu, J. *Phys. Lett. A* **2005**, *341*, 212–215.
(104) Zolin, V. F. *Mol. Phys.* **2004**, *102*, 1377–1380.
(105) Tyeklar, Z.; Dunham, S. U.; Midelfort, K.; Scott, D. M.; Sajiki, H.; Ong, K.; Lauffer, R. B.; Caravan, P.; McMurry, T. J. *Inorg. Chem.* **2007**, *46*, 6621–6631.
(106) Mundoma, C.; Greenbaum, N. L. *Biopolymers* **2003**, *69*, 100–109.
(107) Pasha, A.; Tircso, G.; Benyo, E. T.; Brucher, E.; Sherry, A. D. *Eur. J. Inorg. Chem.* **2007**, 4340–4349.
(108) Cacheris, W. P.; Nickle, S. K.; Sherry, A. D. *Inorg. Chem.* **1987**, *26*, 958–960.
(109) Byegard, J.; Skarnemark, G.; Skalberg, M. *J. Radioanal. Nucl. Chem.* **1999**, *241*, 281–290.

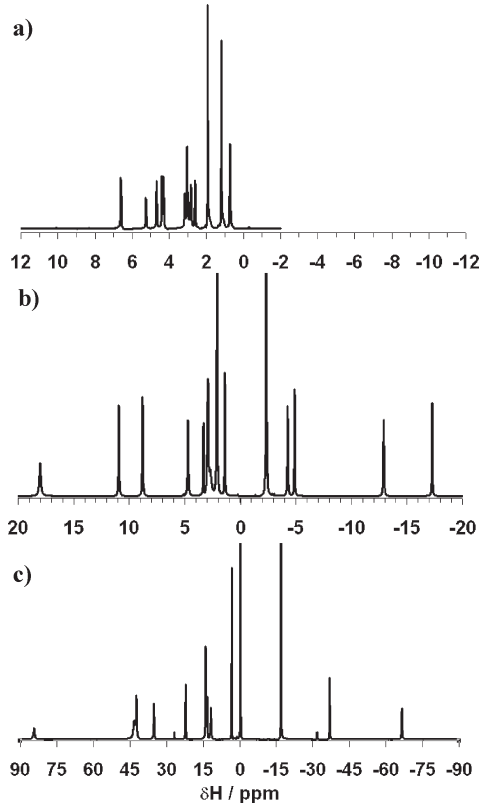


**Figure 7.** $^1$H NMR spectrum of (a) Sm**L**$(NO_3)_3$, (b) Eu**L**$(NO_3)_3$, and (c) Yb**L**$(NO_3)_3$ ($CD_3CN$:$D_2O$, 9:1).

addition of a small amount of $D_2O$ (about 10%) to each sample greatly increased the solubility of the complexes. $^1$H NMR spectra of the three complexes display different amounts of paramagnetic shifting that is consistent with other complexes in the literature. The Yb(III) complex is shifted the most because of stronger dipolar shifting than the other nuclei, while the Sm(III) complex is shifted the least.[110] However, all three complexes display the same number of resonances (14 in 9:1 $CD_3CN/D_2O$ solutions). Attempts to obtain NMR data on the corresponding Gd(III) complex resulted in irresolvable broadened peaks.

Initial assignment of the solution structures was attempted using the diamagnetic lanthanide ion Lu(III). It was found that the *in situ* synthesis of the Lu(III) complex resulted in rapid precipitation resulting from low solubility in organic solvents as well as water. The full assignment presented here was accomplished using the Eu(III) complex (Figure 8), with analogous results for the Sm(III) and Yb(III) complexes (see Supporting Information).

**Assignment of the Eu(III) Complex.** The Eu(III)**L** complex gives rise to broadened signals spread out over an about 40 ppm range. The $^1$H NMR titrations of the ligand with $Eu(NO_3)\cdot 6H_2O$ in $CD_3CN$ indicated the formation of only one species in solution. The complex quickly forms on the NMR time scale, and complete complexation of the ligand can be seen in the NMR spectrum immediately after addition of 1 equiv of $Eu(NO_3)_3$.

In only $CD_3CN$ solvent, there are a total of 16 peaks in the $^1$H spectra while 14 peaks are observed in $CD_3CN/D_2O$

(110) Bertini, I.; Luchinat, C.; Parigi, G. *Solution NMR of Paramagnetic Molecules: Application to Metallobiomolecules and Models*; Elsevier: Amsterdam, 2001.

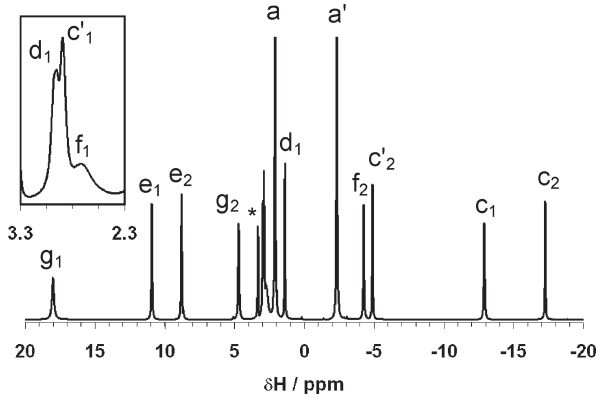


**Figure 8.** $^1$H NMR spectrum of Eu(III)**L** ($CD_3CN/D_2O$ (9:1), 32 °C). The inset shows a higher resolution image of the three peaks at about 3.0 ppm (* is a water peak).

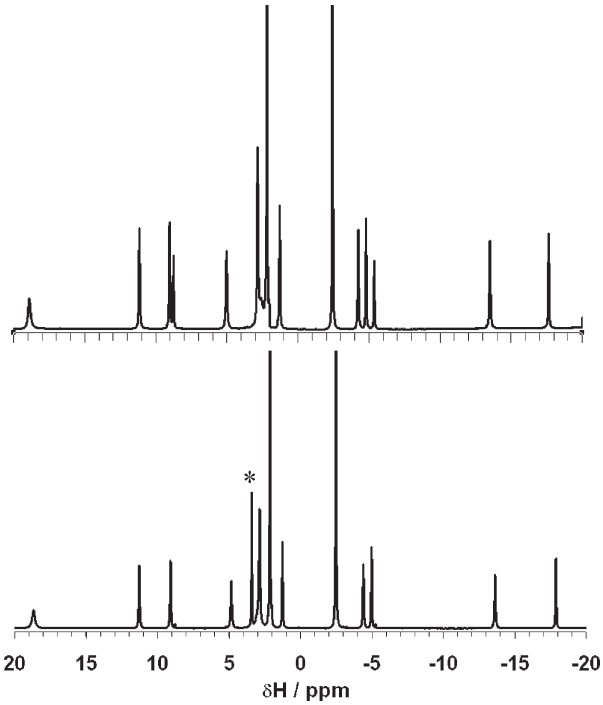


**Figure 9.** $^1$H NMR spectrum of Eu(III)**L** showing the presence of two exchangeable protons at 8.73 and −5.43 ppm after titration with $D_2O$ (Top: $CD_3CN$ only. Bottom: $CD_3CN/D_2O$ (9:1). * denotes solvent).

samples (for the numbering of 16 ligand H's see Scheme 1) because of exchange of the acidic −NH protons with $D_2O$. These are the exact number of resonances that are expected if the complex has $C_2$ symmetry, similar to that observed in the X-ray structure, and if geminal protons are held in inequivalent environments because of Ln(III) ion coordination. The results suggest that the complex is stable on the NMR time scale and resembles a $C_2$ symmetric structure such as that of the X-ray structure.

The proton spectrum shows two large intensity peaks which are assigned as the *t*-butyl protons (Figure 8). These peaks show up at about 2.0 and −2.5 ppm and have the narrowest line width and longest $T_1$ times as would be expected from the protons furthest away from the paramagnetic ion. The assignment of the −NH protons was based on the chemical exchange and disappearance with $D_2O$ addition (Figure 9). The presence of two

unique −NH environments is also consistent with the complex having a $C_2$ symmetry axis on the NMR time scale. The complete assignment of the remaining protons in the $^1$H NMR spectrum is shown in Figure 8. This assignment is based on the results of the COSY and HMQC experiments discussed in the two-dimensional NMR section below.

The $^{13}$C NMR spectrum of the Eu(III) complex is also in agreement with the symmetry suggested by both the X-ray crystal structure and the proton NMR. There are 12 resonances seen in the $^{13}$C NMR (Figure 10). Two large resonances are found for the *t*-butyl carbons as well as two different carbonyl peaks. These were confirmed by the APT (data not shown), DEPT (not shown), and HMQC (see below) experiments. The remaining $CH_2$ carbon resonances were assigned using the results from the 2D NMR experiments (see below).

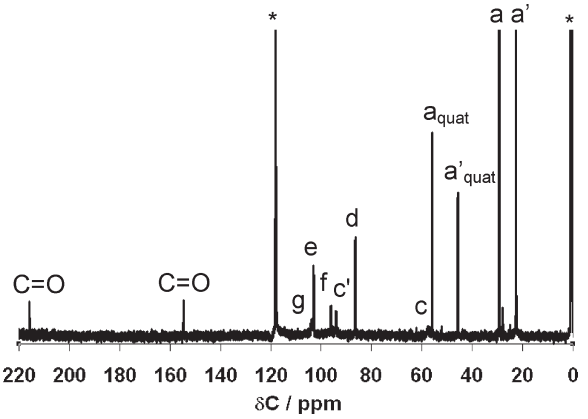


**Figure 10.** $^{13}$C NMR spectrum of Eu(III)**L** in $CD_3CN/D_2O$, 9:1 (* indicates solvent).

**Two-Dimensional NMR Characterization.** The COSY NMR spectrum of the Eu(III) complex (Figure 11) shows both 1-bond (geminal) and 2-bond (vicinal) couplings between $-CH_2-$ protons. Four sets of related protons are observed: two sets of inequivalent ether $-CH_2-CH_2-$ groups and two inequivalent amide $-CH_2-$ groups. The first $-CH_2-CH_2-$ group can be found by starting with proton $g_1$ and relating it through the off-diagonal peaks to the $g_2$ and $f_2$ protons, correlating the three related protons. The fourth proton to complete the group is the $f_1$ proton. No coupling is seen between the $g_1$ and $f_1$ protons; however, coupling between the $f_1$ and $f_2$ protons is observed showing that the $f_1$ proton is part of this group. This set of $-CH_2-CH_2-$ protons is more highly paramagnetically shifted than the other related proton groups and could explain the difficulty in observing the 2-bond coupling between the $f_1$ and neighboring protons. The second $-CH_2-CH_2-$ group is better resolved and shows three off-diagonal peaks for each proton. Starting with the $e_1$ proton at about 11 ppm, cross-peaks couple this proton to the $e_2$ and the $d_{1,2}$ protons, thus correlating all four protons in the group with one another.

The two pairs of inequivalent amide $-CH_2-$ protons display only one cross peak consistent with the geminal coupling to the only nearby proton. These two pairs of protons are labeled $c_{1,2}$ and $c'_{1,2}$. Using the COSY spectrum it is possible to determine couplings between protons but not which couplings arise from 1- or 2-bond couplings. The HMQC experiment was used to determine which couplings seen in the COSY spectra arise from 1-bond couplings and confirm the assignment proposed in Scheme 1.

The HMQC NMR spectrum (Figure 12) shows two proton peaks for every carbon peak, except for the *t*-butyl peaks at about 22 and 28 ppm on the $^{13}$C axis. The intensity of the $g_1$ proton (Figure 13, ca.18 ppm) is very

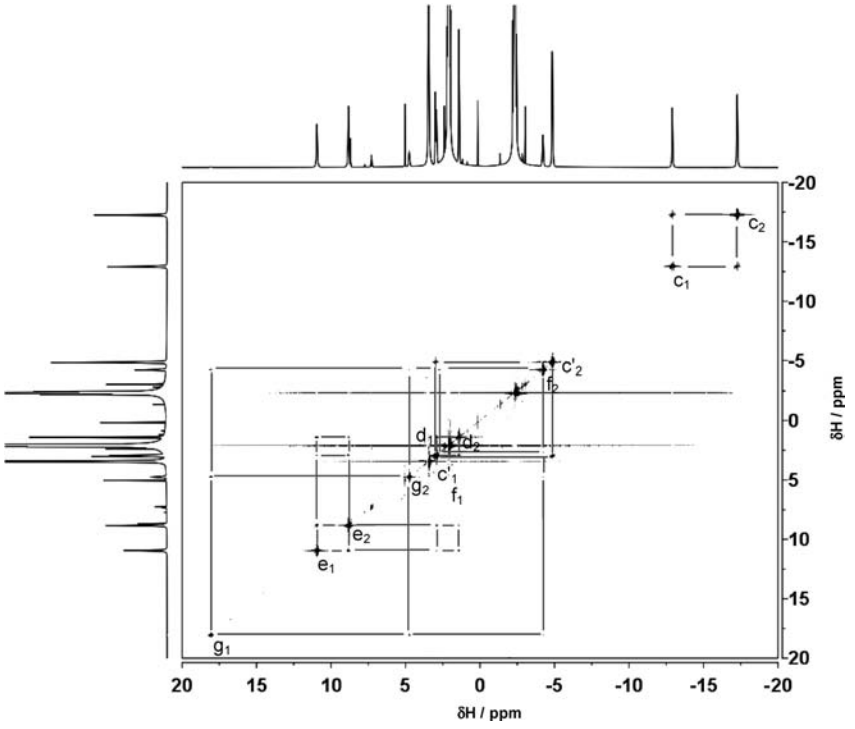


**Figure 11.** COSY spectrum of Eu(III)**L** ($CD_3CN/D_2O$, 9:1, 32 °C). Lines connecting cross peaks were added for clarity.

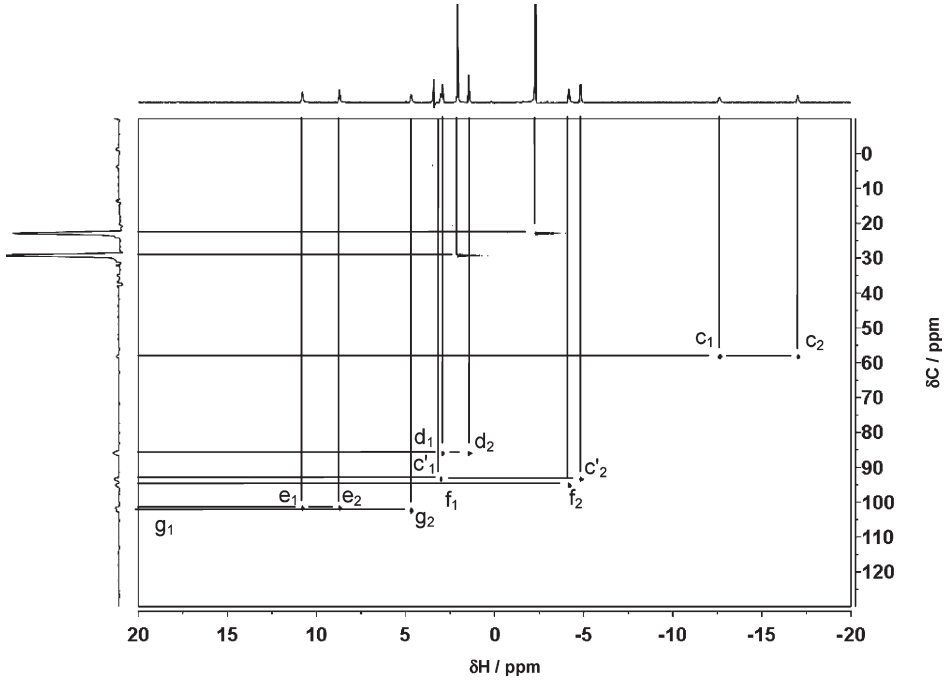


**Figure 12.** HMQC spectrum of Eu(III)**L** ($CD_3CN/D_2O$, 9:1, 25 °C). The positions of the $g_1$ and $f_1$ protons are labeled but not visible. Lines connecting cross peaks were added for clarity.

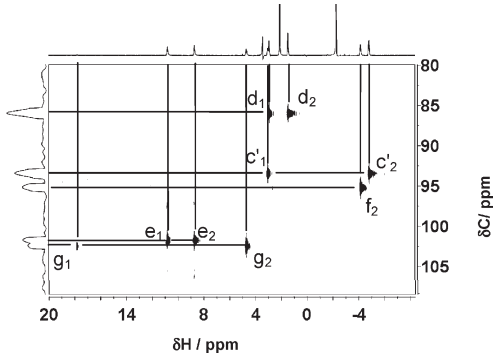


**Figure 13.** Close up view of the HMQC spectrum of Eu(III)**L** showing the location of the $g_1$ proton ($CD_3CN/D_2O$, 9:1, 25 °C). Lines connecting cross peaks were added for clarity.

weak and is only seen when the spectrum is processed with a much lower contour threshold. The spectrum identifies the 1-bond couplings between the $g_{1,2}$, $e_{1,2}$, $d_{1,2}$, $c_{1,2}$, and $c'_{1,2}$ protons. There is a peak missing for the $f_1$ proton as in the COSY spectrum, perhaps due again to its proximity to the paramagnetic metal center.

**PARACEST Experiments.** Paramagnetic chemical exchange saturation transfer (PARACEST) agents[111] have recently been used for a number of different imaging applications. They can be useful for pH mapping of tissues by taking advantage of the pH dependent properties of the exchangeable proton site.[22] Aime et al. demonstrated that arylsulfonamide derivatives of cyclen type macrocycles have a very strong pH dependence.[12] There are also reagents that exploit interactions between the complex and metabolites or proteins. For example, PARACEST complexes have been specifically designed to bind to the active site of enzymes,[12,24] or detect the presence of certain metabolites such as glucose,[25] glycogen,[26] or phosphate esters.[27] Some reagents can also detect metal ions, such as copper[112] and zinc.[113] Many PARACEST reagents are made using a derivative of DOTA or other similar macrocycles. Amide derivatives of the DOTA ligand have been shown to decrease the bulk water signal through CEST by up to 60%.[21] Given the presence of acidic protons on the amide groups of our new ligand **L**, we were interested in exploring the CEST properties of its corresponding complexes.

PARACEST NMR experiments were preformed on the Eu(III) complex to determine its viability as an MRI contrast reagent. Experiments using Gd(III), the lanthanide ion popular with MRI, were not possible given the large paramagnetic peak broadening of the protons on the ligand and resulting unresolved amide peaks (data not shown). Samples of the Eu(III) complex were tested at pH 4, 7, and 9 and at temperatures ranging from 5 to 85 °C. It was found that the exchange at pH 4 was too slow to observe any CEST peaks. In samples at pH 9 the exchangeable −NH proton signals were not present because of rapid exchange on the NMR time scale or complete deprotonation, and no CEST peaks were detected in this sample.

At pH 7 there were CEST peaks present in the spectrum resulting from the exchangeable amide −NH protons at temperatures ranging from 5 to 85 °C. The CEST spectrum at 37 °C is shown in Figure 14. As would be expected from the two inequivalent −NH groups, the spectrum shows two regions at about −4.8 and 9.5 ppm where a decrease in the intensity of the bulk water peak is observed upon their saturation. The location of these two

(111) Sherry, A. D.; Woods, M. *Annu. Rev. Biomed. Eng.* **2008**, *10*, 391–411.

(112) Que, E. L.; Chang, C. J. *J. Am. Chem. Soc.* **2006**, *128*, 15942–15943.

(113) Major, J. L.; Parigi, G.; Luchinat, C.; Meade, T. J. *Proc. Natl. Acad. Sci. U.S.A.* **2007**, *104*, 13881–13886.

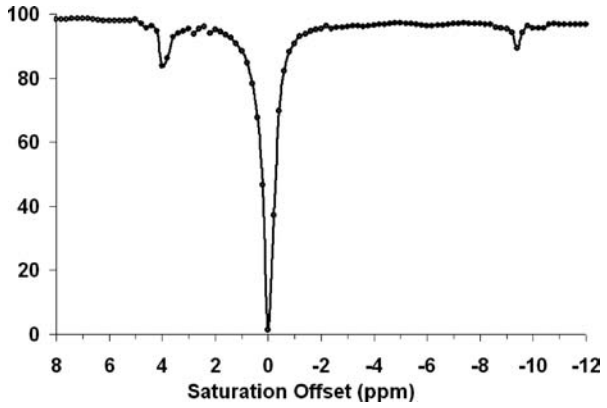


**Figure 14.** PARACEST spectrum of Eu(III)**L** complex (75 mM) recorded in $H_2O$ at 500 MHz, 37 °C, and pH 7.0.

CEST peaks corresponds to the location of the exchangeable −NH protons found in the NMR spectrum (Figure 9) after considering the small shift in the −NH peaks because of the temperature differences between the two spectra. The decrease in the water peak intensity was found to be 16% when saturating the −NH proton that is 4.0 ppm and 10% when saturating the other −NH proton that is −9.4 ppm from the bulk water signal. The difference in the effectiveness of these two peaks could be caused by the two inequivalent −NH peaks having slightly different exchange rates. The peak at −9.4 ppm appears sharper than the 4.0 ppm peak. This suggests that the −9.4 ppm peak has a slower exchange rate than the 4.0 ppm −NH proton and therefore possibly a less effective saturation transfer at 37 °C in water.[21]

## Conclusions

We report the design and synthesis of a new polydentate amide ligand and examined its coordination to lanthanide ions. The design of this ligand allows ready modification of R-groups to change its solubility characteristics or exploit different properties of the Ln(III) ion. Complexes of **L** with Sm(III), Eu(III), and Yb(III) were analyzed in the solid state by X-ray crystallography. The structure of the nine-coordinate complexes were characterized by the methods of Guggenberger and Muetterties[60] and found to be distorted tricapped trigonal prismatic. The structures had mostly normal bond distances with the exception of consistently shorter Ln(III)−O ether bond distances when compared to predominantly Ln(III) crown ether complexes. Also, average distances across the complexes decreased in a fashion consistent with the expected decrease in ionic radii in moving from left to right across the lanthanide series.

The ligand was weakly absorbing, and luminescence was observed by directly exciting the metal ion. Luminescence spectra of solution and solid state samples supported similar structures. The IR spectra showed carbonyl and ether peaks shifted to lower energy and were consistent with free uncoordinated nitrate counterions, consistent with the X-ray data. The solution structures were analyzed using 1D and 2D NMR experiments. The presence of 16 resonances in the 1D $^1$H NMR spectrum provided strong support that the complexes are assembled in solution with a $C_2$ symmetry axis similar to that observed in the crystal structures. NMR titration experiments using $CD_3CN/D_2O$ confirm that the complex has two exchangeable proton sites corresponding to two sets of nonequivalent amide −NH protons. This behavior was consistent with X-ray and MS data that are consistent with acidic amide protons.

The presence of acidic and readily exchangeable protons on the ligand in the complex allowed us to observe CEST phenomenon. The PARACEST experiments with the Eu(III) complex showed two CEST peaks at the same location as the two exchangeable −NH protons. Saturation at these locations causes a decrease in the bulk water molecule signal intensity of 10 and 16%. Furthermore, the ITC data allowed the determination of binding constants for the complex of $\log K \sim 9.5$, which is not as high as complexes of similar carboxylic acid containing chelates. These data characterize a chelating amide containing ligand as a possibly useful class of CEST agents in the exploration for new and improved imaging reagents.

**Acknowledgment.** S.M.B is grateful to the Research Corporation (Grant CC6396), the Swenson Family Foundation, and UMD for financially supporting this research. J.D.D. thanks the UMD Department of Chemistry for a Moses Passer Fellowship. R.D.P. is indebted to NSF (CHE-0443345) and the College of William and Mary for the purchase of the X-ray diffraction equipment. The authors would like to thank Dr. Beverly Ostrowski for assistance with NMR and Mr. Kris Knutson and Dr. Anne Hinderliter for assistance with ITC experiments.

**Supporting Information Available:** Crystallographic data for the three Ln(III) complexes in CIF form. Mass spectrometry data and $^1$H, $^{13}$C, HMQC, and COSY NMR spectra for the Sm(III) and Yb(III) complexes. ITC data used for the Eu(III) complex binding studies. This material is available free of charge via the Internet at http://pubs.acs.org.